

# PyRaysum: Software for Modeling Ray-theoretical Plane Body-wave Propagation in Dipping Anisotropic Media

Wasja Bloch <sup>\* 1</sup>, Pascal Audet <sup>2</sup>

<sup>1</sup>Department of Earth, Atmospheric and Ocean Sciences, University of British Columbia, Vancouver, BC, Canada, <sup>2</sup>Department of Earth and Environmental Sciences, University of Ottawa, Ottawa, Ontario, Canada

Author contributions: *Writing, Software:* W. Bloch, P. Audet. *Visualization, Validation:* W. Bloch. *Conceptualization:* P. Audet.

**Abstract** This article introduces *PyRaysum*, a Python software for modeling ray-theoretical body-wave propagation in dipping and/or anisotropic layered media based on the popular Fortran code *Raysum*. We improve and expand upon *Raysum* in several ways: 1) we significantly reduce the overhead by avoiding input/output operations; 2) we implement automatic phase labeling to facilitate the interpretation of complex seismograms; 3) we provide the means to correct inaccuracies in the calculated amplitude of free surface reverberations. We take advantage of the modern, object-oriented Python environment to offer various classes and methods to perform receiver function calculation, filtering and plotting. *PyRaysum* is fully backward compatible with legacy *Raysum* files and integrates well with *NumPy* and *ObsPy*, two standard libraries for numerical computing and seismology. *PyRaysum* is built in Python version 3 and requires a Fortran compiler, but otherwise runs on all platforms. The software offers a high-level, ease-of-use user interface and is equipped with complete documentation and testing as well as tutorials to reproduce published examples from the literature. Time-optimized post-processing functions allow for the straightforward and efficient incorporation of *PyRaysum* synthetic data into optimization or probabilistic parametric search approaches.

**Non-technical summary** We introduce *PyRaysum*, an overhaul of the popular Fortran computer program *Raysum* for modeling receiver functions, wrapped in the python programming language. *PyRaysum* computes synthetic seismograms for subsurface models that consist of a few layers with constant elastic properties. The layer properties may be anisotropic and the layers may be dipping. Compared to the original code, *PyRaysum* is faster, more intuitive to use, and can easily be combined with other programs written in the Python programming language. These enhancements facilitate its usage in the estimation of subsurface properties from seismograms.

## 1 Motivation

Modeling teleseismic body-wave propagation in complex media is an important component of passive seismological approaches that aim to decipher upper mantle and crustal seismic velocity structure on the receiver side (e.g., receiver functions and teleseismic shear-wave splitting analyses). Modeling wave propagation in highly heterogeneous and anisotropic 3D media can be performed using full-waveform approaches (e.g. spectral element or finite-difference methods). Most often, however, a simpler parameterization of the subsurface velocity structure is desirable, because Earth structure is dominantly 1D or 2D at the scale of the upper mantle and lithosphere, and faster modeling methods allow searching for a wider range of model parameters that fit the data. Among those approaches,

matrix-propagation techniques (Kennett, 2009; Thomson, 1997) provide accurate wave field reconstructions from horizontally layered media, including anisotropy. However, heterogeneous seismic velocity structure, in the form of layer dip (Figure 1), is not easily incorporated in such approaches. The most popular alternative for modeling layer dip (with or without layer anisotropy) is based on a ray-theoretical approximation that can model low-order scattering, but neglects higher order wave effects (Cassidy and Ellis, 1993; Frederiksen and Bostock, 2000). This approach is implemented in the software *Raysum* (Frederiksen and Bostock, 2000), which has been used in numerous receiver function studies to characterize seismic discontinuities such as the continental Moho (e.g., Lombardi et al., 2008), the lithosphere-asthenosphere boundary (e.g., Kumar et al., 2007), or the mid-lithosphere discontinuity (e.g., Selway et al., 2015), and has helped unravel the

\*Corresponding author: wbloch@eoas.ubc.ca

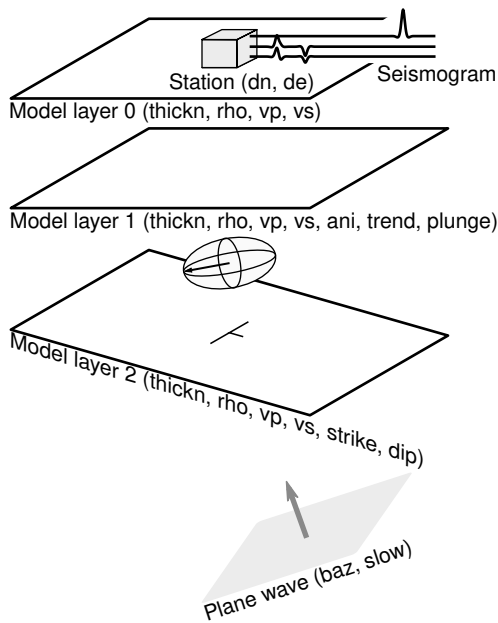


**Figure 1** *PyRaysum* computes three-component synthetic seismograms for a plane wave that travels through a stack of dipping, anisotropic layers. This example shows a 2-layer over a half-space model, where the top and bottom layers are isotropic, and the middle layer is elastically anisotropic (represented by the anisotropic ellipsoid (*ani*) and orientation (*plunge* and *trend*) of the symmetry axis). The top interface of the half-space is inclined, as parameterized by the *strike* and *dip* angles. The ray geometry is defined by the back-azimuth and horizontal slowness of the incident plane wave ray vector and the location of the station relative to the origin.

seismic velocity structure within subduction zones (e.g., Audet and Bürgmann, 2014; Nicholson et al., 2005), orogenic belts (e.g., Schulte-Pelkum et al., 2005; Sodoudi et al., 2009), and collisional settings (Schneider et al., 2013).

The original *Raysum* software is written in native Fortran for fast and efficient computations. The input and output to *Raysum* consist of formatted text files, and users have to write their own scripts for reading, writing, processing and visualizing the synthetic data. This makes it challenging and cumbersome for beginners to quickly produce synthetic data, explore the parameter space efficiently, and combine synthetic with observed data in optimization problems. Furthermore, reading and writing files to disk represent a substantial performance bottleneck for repeated and automated program execution. *PyRaysum* was developed to remedy these shortcomings, by wrapping *Raysum* in a modern Python environment with classes and modules to facilitate its usage for beginners and to streamline the modeling approach in optimization or probabilistic search approaches. It employs *ObsPy* (Krischer et al., 2015) for handling seismic data, *NumPy* (Harris et al., 2020) for data processing, and *Matplotlib* (Hunter, 2007) for visualization. The installation, testing, full user interface and Jupyter notebook tutorials are described in the online documentation at <https://paudetseis.>

**Listing 1** General structure of a *PyRaysum* setup. The parameters chosen here reproduce the synthetic data shown in Figure 2.

```
from pyraysum import Model, Geometry, Control
from pyraysum import run
from fraysum import run_bare

# Subsurface model
mod1 = Model(
    thickn=[32000, 0], # m
    rho=[2800, 3600], # kg/m^3
    vp=[6400, 8100], # m/s
    vs=[3600, 4650], # m/s
)

# Ray geometry
geom1 = Geometry(
    baz=97, # degree
    slow=0.07, # s/km
)

# Run-control parameters
ctrl1 = Control(
    mults=2, rot="ZNE", npts=1000, align=0
)

# Result with ObsPy Streams
res1 = run(mod1, geom1, ctrl1)

# NumPy Array
arr1 = run_bare(
    *mod1.parameters,
    *geom1.parameters,
    *ctrl1.parameters,
)
```

[github.io/PyRaysum/index.html](https://github.io/PyRaysum/index.html). Here we give an overview of the user interface and provide examples that validate the results against published and synthetic examples. We provide timing benchmarks for various program execution options and suggest new applications that arise from the improved performance and transparency of results.

## 2 User Interface

Simulating seismic waveforms with *PyRaysum* is done by setting up: 1) a subsurface model; 2) the ray and station geometry; and 3) a suite of run-control parameters. With this setup, synthetic seismograms can either be generated as *ObsPy* Streams or *NumPy* arrays. In Listing 1, the *res1* and *arr1* objects both contain the same synthetic seismograms. They differ in that *res1* is a *Result* object that contains the synthetics as feature-rich *ObsPy* Streams with additional metadata, while *arr1* holds the bare synthetic samples as a *NumPy* Array. *PyRaysum* offers common methods for receiver function post-processing for both objects, where the *ObsPy*-based routines focus on exploratory data analysis, while the *NumPy*-based ones have an emphasis on computational efficiency.

*PyRaysum* provides two packages: *fraysum* and *pyraysum*. *fraysum* bundles access to the underlying Fortran routines, which are based on the original *Raysum* code (Frederiksen and Bostock, 2000).

pyraysum provides the Python interface for computing, post-processing and plotting receiver functions. The object-oriented interface can be imported directly from `pyraysum`. Functions for advanced users are stored in three modules: `prs` allows users to create `PyRaysum` objects from files, including legacy `Raysum` files; `frs` exposes functions for fast, `NumPy`-based post-processing of `fraysum` output; `plot` provides plotting functionality.

## 2.1 fraysum

The `fraysum` package is generated during compilation of the `Raysum` code through the `NumPy` `f2py` interface generator. This package facilitates access to the `run_full()` and `run_bare()` functions, which are the low-level calls to the underlying Fortran code. `run_bare()` only returns the synthetic 3-component seismograms, while `run_full()` additionally returns arrays of times, amplitudes and identifiers of the converted and reflected seismic phases, at the cost of a longer run time. This module lacks any convenience and bookkeeping functionality.

## 2.2 pyraysum

The `pyraysum` package exposes the primary function `run()` to compute synthetic seismograms. It defines the three classes `Model`, `Geometry` and `Control` that organize the required input parameters and the `Result` class that holds the results.

**run()** Results are created through a call to `run()`, which requires an instance of each input parameter classes representing a subsurface model (`Model`), the ray- and station geometry (`Geometry`) and run control parameters (`Control`) as required positional arguments. The optional keyword arguments `rf` and `mode` provide switches to automatically compute receiver functions and skip automatic phase labelling.

**Model** The subsurface seismic velocity structure is parameterized as a stack of layers (Figure 1), where each layer is described by its vertical thickness (`thickn`, in  $m$ ), density (`rho`, in  $kg/m^3$ ) and isotropic P- and S-wave velocities (`vp` and `vs`, in  $m/s$ ), indexed from top to bottom. Optionally, the layer may be inclined (`strike` and `dip` angles in degrees with a right-hand-rule) and/or anisotropic (`ani` is percent anisotropy; Figure 1). Anisotropy is parameterized in a simplified hexagonal symmetry class as

$$ani = \frac{V_{\parallel} - V_{\perp}}{V} \cdot 100\%, \quad (1)$$

where  $V_{\parallel}$  and  $V_{\perp}$  are the seismic velocities parallel and perpendicular to the symmetry axis. P- and S-wave anisotropy are equal and pure elliptical anisotropy is assumed (Porter et al., 2011; Sherrington et al., 2004; Levin and Park, 1997). The orientation of the anisotropy axis is defined by `plunge` (degrees down from horizontal) and `trend` (degrees clockwise from north) angles. Positive anisotropy refers to a fast axis of symmetry, whereas

negative anisotropy denotes a slow axis. We note that, unlike all other model parameters that apply to the entire layer properties, specifying layer strike and dip angles refers to the orientation of the top interface. To define a uniform-thickness dipping layer, the same strike and dip angles must be specified at the underlying layer.

The model layers can be accessed and manipulated by their index (see Section 3.2 for examples). Convenience methods for the manipulation of a `Model` instance include: parametrizing `vp` and `vs` in terms of  $V_P/V_S$  (`vpvs`); changing model attributes interactively using brief command strings (`change()`); adding, splitting, removing and averaging of layers (`+`, `split_layer()`, `remove_layer()`, `average_layer()`); plotting the subsurface model as a staircase diagram or profile sketch (`plot()`); saving the model to file, including legacy `Raysum` model files (`save()`).

**Geometry** The ray and station geometry are parameterized in terms of the ray back-azimuth angle (`baz`, in degrees clockwise from north) and horizontal slowness (`slow`, in  $s/km$ ), and station offset in north and east direction from the model origin (`dn` and `de`, in  $m$ ). Ray parameters can be specified as either floats to model single-event waveforms, or iterables to simulate multiple event recordings. Each ray can be accessed and manipulated by index, where the ray indices are associated with those of the three-component synthetic waveforms in the `Result` object generated from a call to `run()` (see below).

**Control** The `Control` class controls the computation of the synthetic waveforms. Various options can be specified, namely: the number of samples (`npts`) and the sampling interval (`dt` in  $s$ ) of the seismograms; the polarization of the incoming wave-field (`wvtype`); the order to which free surface reverberations are computed (`multples`, `mults`); whether only specific phases should be computed (`set_phaselist`); the time-alignment (`align`) and time-shift (`shift`) of the seismograms; the rotation of seismogram components to left-handed geographical (Z-N-E) or right-handed ray (R-T-Z or P-V-H) coordinate systems (`rot`); and the verbosity of the program execution (`verbose`). Default options exist for each of these parameters.

**Result** The `Result` class holds the output synthetic seismograms, which can be accessed by ray index or as a list of 3-component `ObsPy` Streams with the `"stream"` or `"seismogram"` keyword. If the seismograms are computed in a ray coordinate system (`rot` equal to `"RTZ"` or `"PVH"`), synthetic receiver functions can be computed on the fly using the `calculate_rfs()` method. They are then stored as an additional list of 2-component (radial/vertical shear and transverse/horizontal shear) `ObsPy` Stream objects under the `"rf"` keyword and can be accessed as the second element of the returned tuple when indexing `Result`. All functionalities of the `ObsPy` Stream class are readily available. Convenience methods `plot()` and `filter()` allow plotting and filtering the `streams` or `rfs` attributes in a single command.

The arrival time, amplitude, phase descriptor, abbreviated phase name, and conversion name of each converted or reflected phase arrival are stored within the `stats` attribute for each trace within the seismogram streams. The `phase_descriptors` serve as unique phase identifiers throughout `PyRaysum`. They are strings that consist of paired indices and letters that fully describe the direction (up or down) and type of rays converted or reflected at specific interfaces. *P* indicates a P-wave, *S* a (fast) S-wave and *T* a (slow) S-wave. Uppercase and lowercase letters indicate up-going and down-going rays, respectively. In the case of an isotropic medium, *S* and *T* arrive at the same time and may both carry some energy. Note that *S* and *T* do not imply a polarization, but are chosen as synonyms for *S1* and *S2* to avoid ambiguity with the layer indices. For instance, the phase descriptor of the P-to-S converted wave at the bottom of the top-most layer (index 0) in a 2-layer over half space model (Figure 1) would be *2P1POS*. The `conversion_names` attribute abbreviates the phase descriptors by omitting equal wave types in adjacent ray segments, only indicating the layer indices on top of which a conversion has occurred. The conversion name of the example phase would be *P1S*. Lastly, the `phase_names` attribute provides the shortest, yet ambiguous phase description, listing only the converted phase types, here *PS*. The unique set of all phases present can be retrieved with the `descriptors()` method.

### 2.2.1 prs

The `prs` module holds the object-oriented interface described above and additional functions to interact with it. Namely, `read_geometry()`, `read_control()`, and `read_model()` read saved input objects from file and allow the direct use of legacy `Raysum` files. `equivalent_phases()` returns the seismic phases that arrive at the same time as a given phase (see Section 4).

### 2.2.2 frs

The `frs` module holds the functions used to interpret `fraysum` output. Most importantly, `make_array()` allocates an array suitable for the repeated post-processing of similar waveform simulations. Post-processing can be done with `filtered_array()` and `filtered_rf_array()`, the `NumPy`-based, computationally-efficient functions to compute filtered synthetic seismograms and receiver functions from the output of `fraysum.run_bare()`.

### 2.2.3 plot

The `plot` module holds the plotting functions used by the `Result.plot()` method. The direct function calls expose more options to customize the plots. `stream_wiggles()` and `rf_wiggles()` create plots of multiple-event seismograms or receiver functions with either 3- or 2-component panels, respectively, ordered by either back-azimuth or slowness. The function `seis_wiggles()` creates a line plot of single-event seismograms.

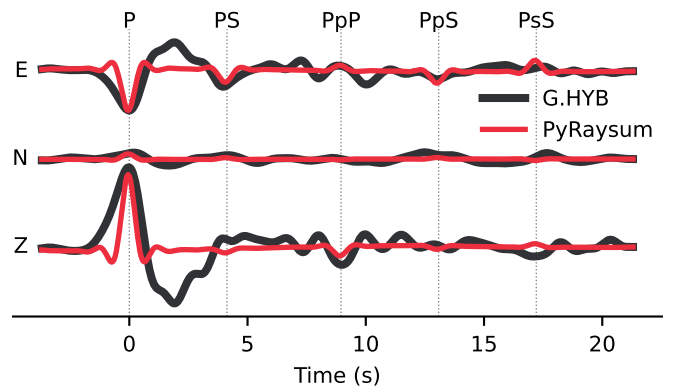


**Figure 2** Modeling of the direct Moho conversion and multiples of a teleseismic seismogram recorded at station *G.HYB*. The code that generates the impulse response function is given in Listing 1. The P-to-S Moho conversion *PS*, as well as its free surface reverberations *PpP*, *PpS*, and *PsS* modeled on the basis of the subsurface model of [Saul et al. \(2000\)](#) are discernible in the seismogram. Model and Data traces were bandpass filtered between 1 and 20 s and scaled to the *P* amplitude on the east-component.

## 3 Examples

In this section, we present three simple workflows that showcase usage of `PyRaysum`: In Section 3.1 we forward model three-component waveforms through a simple layer-over-half-space model and compare them with observed data at station *G.HYB* in Hyderabad, India; in Section 3.2 we demonstrate how to interactively manipulate models and quickly examine the resulting receiver function signature; and in Section 3.3 we reproduce previously published synthetic receiver functions representative for coastal California, USA, where a strongly anisotropic layer underlies a crustal block.

### 3.1 Conversions and multiples in a Seismogram

Station *G.HYB* is located on a seismically transparent cratonic crust. It yields very clear receiver function data ([Saul et al., 2000](#)) that show the direct P-to-S Moho conversion (*PS*) and first-order free-surface reverberations (*PpS* and *PsS*) arriving  $\sim 4$  s,  $\sim 12$  s and  $\sim 16$  s after the direct P-wave, respectively. These data are consistent with a 33 km-thick crust with an average S-wave velocity  $V_S$  of 3.7 km/s and a P-to-S wave velocity ratio  $V_P/V_S$  of 1.74 ([Saul et al., 2000](#)).

Here we use seismic data recorded at station *G.HYB* for a magnitude *M* 6.3 earthquake that occurred on January 1, 2002 in the Philippines, as a test case for waveform modeling. This wave front arrives due east at the station, and its direct P-waveform exhibits a relatively simple, Ricker-II-like shape due to the large earthquake focal depth (140 km; Figure 2). We model these three-component waveforms with `PyRaysum` (Listing 1) using the appropriate source-receiver geometry and the seismic velocity model proposed by [Saul et al. \(2000\)](#). In the `Control` parameters, no time alignment (`align=0`) is applied and we specify a geographic coordinate system (`rot="ZNE"`). The synthetic waveforms reproduce

the main phase arrivals, although the convolved source wavelet distorts this comparison. The phase names, times and amplitudes are the `phase_names` output by `PyRaysum` and facilitate the understanding and description of seismograms. A more complete example is part of the online `PyRaysum` documentation.

### 3.2 Interactive exploration of receiver functions

We next demonstrate how the effect of changes in the subsurface structure on receiver functions can be explored. In Listing 2, we specify rays with evenly spaced back-azimuths and a constant horizontal slowness of  $0.06 \text{ s km}^{-1}$ . We set the rotation of the coordinate axes to the P-V-H system, which are oriented parallel to the  $P$ -,  $SH$ -, and  $SV$  polarization of the incoming wave field as predicted by the ray back-azimuth, slowness, and isotropic velocities of the topmost model layer (Kennett, 1991). This rotation ensures that as much converted energy as possible is mapped to the radial and transverse components and removes the constant-amplitude, zero-lag signal on the radial component. Receiver function calculation is straightforward with a simple argument `rf=True` in the call to `run()`. Figure 3a shows the receiver function signature of the isotropic crust modeled in the previous example with a horizontal Moho as the only interface. The  $PS$ -conversion is clearly visible on the radial component at 4 s.

To explore the effect of a possible dipping Moho, we next set a  $30^\circ$  eastward dip of the interface (Listing 2 and Figure 3b). The effect is an undulation of the Moho conversion in timing and amplitude with a period of  $360^\circ$  (so-called  $1-\theta$  variations). Converted waves from the west arrive earlier and with a lower amplitude on the radial component, due to the relatively shorter ray path and lower layer-orthogonal incidence angle. Conversely, conversions from the east arrive later and with a higher amplitude. Energy from northerly and southerly directions gets converted into the dip direction, evident from the positive and negative amplitudes on the transverse component. The P-coordinate vector is not aligned with the actual ray polarization, because the dipping interface results in an apparent slowness of the ray that is different from the actual slowness of the layer. Therefore, some energy appears on the radial and transverse components at time 0 s.

Next we rotate the interface by  $180^\circ$ —so that it dips west—and increase its dip to  $60^\circ$  (Listing 2 and Figure 3c), thus producing an interface orthogonal to that in the previous example. The undulation pattern of the conversion is more pronounced between 2 and 3 s. The greater misalignment of the P-coordinate vector with the ray polarization leads to significant converted energy on the P-component that gets mapped to the receiver function as an artificial secondary pulse between 4 and 6 s through deconvolution.

To explore anisotropy in the topmost layer, we set the layer dip back to horizontal and instead vary the anisotropic parameters in the model (Listing 2 and Figure 3d and e). With a fast symmetry axis (orthogonal to plane of slow axes) trending northward and plunging

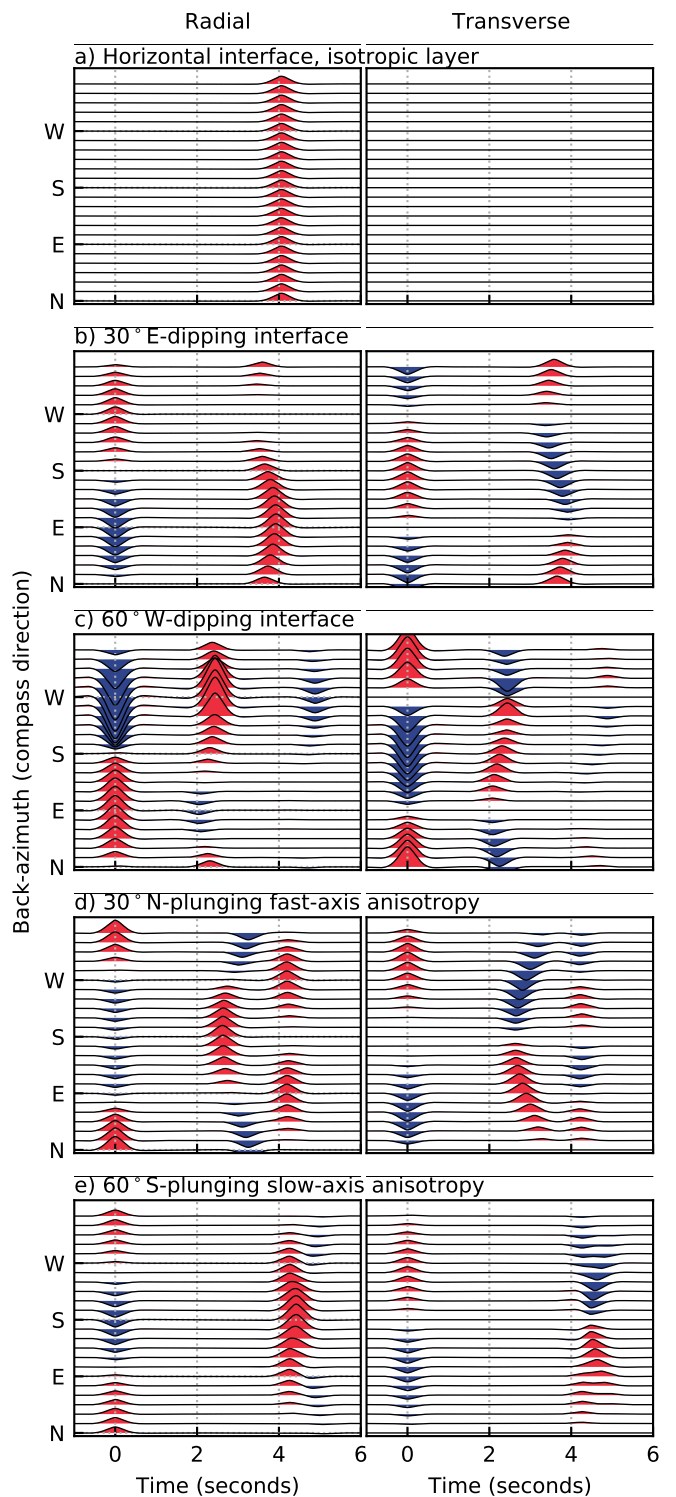


**Figure 3** Interactive exploration of receiver functions. The sections correspond to simple layer-over-half-space subsurface models. An interpretation is given in Section 3.2. The code to produce the images is given in Listing 2.

$30^\circ$ , the converted wave field gets separated into a fast  $S1$ -wave—arriving earlier, N-S-polarized parallel to the fast anisotropy axis, with a strong move-out pattern—and a slow  $S2$ -wave, arriving later, E-W-polarized, without a move-out pattern characterized by  $180^\circ$  periodicity (i.e.,  $2-\theta$  variations). Next we switch from fast- to slow-axis anisotropy and rotate the now unique slow anisotropy axis such that it is aligned with one of the in-

clined slow anisotropy axes from the previous example (Listing 2 and Figure 3e). The polarization of the  $S1$  and  $S2$  waves remains the same. Now the  $S2$ -wave shows the move-out pattern, as the wave encounters azimuthally-varying velocities.

**Listing 2** Exploration of simple layer-over-half-space models with either a dipping interface or anisotropy. Definitions of Listing 1 are assumed.

```
# Plotting parameters
scale = 4000
tmin = -1
tmax = 6

# Evenly spaced back-azimuths, fixed slowness
geom2 = Geometry(range(0, 360, 15), 0.06)

# Create a copy of mod1
model = mod1.copy()

# Direct conversions, PVH coordinate system
ctrl2 = Control(
    mults=0, rot="PVH", dt=0.01, npts=1200
)

# Calculate, filter and plot
# receiver functions
def run_plot():
    res = run(model, geom2, ctrl2, rf=True)
    res.filter(
        "rfs", "lowpass", freq=1,
        zerophase=True, corners=2
    )
    res.plot_rfs(scale, tmin, tmax)

# Figure 3a
run_plot()

# Figure 3b - 30 deg east-dipping interface
model[1, "dip"] = 30
run_plot()

# Figure 3c - 60 deg west-dipping interface
model[1, "strike"] = 180
model[1, "dip"] = 60
run_plot()

# Figure 3d - remove dip, add north-plunging
# fast axis with 20% anisotropy
model[1, "dip"] = 0
model[0, "ani"] = 20
model[0, "plunge"] = 30
run_plot()

# Figure 3e - south-plunging slow axis
model[0, "ani"] *= -1
model[0, "trend"] += 180
model[0, "plunge"] += 30
run_plot()
```

### 3.3 Reproduction of earlier work

To demonstrate the handling of layer dip and anisotropy in multi-layered models and show additional plotting functionality of *PyRaysum*, we reproduce figure 3 of Porter et al. (2011). In Listing 3, the definition of the dipping lower-crustal layer model `dipm` implies that the top of the half space and that of the lower layer are dipping 20°, striking east. The layers of the anisotropic model `anim` are flat. The bottom layer is characterized

by 20% hexagonal anisotropy with a slow symmetry axis (`ani[1] = -20.`) trending south, and plunging 45° down from horizontal. The layer configuration is visualized in Figure 4 a and b, which is a modified output of the call to `model.plot_interfaces()` shown in Listing 3. The corresponding radial and transverse receiver functions are shown in Figure 4c and d, which are plotted using `res.plot('rfs')` with additional options. The complete example is included in the online *PyRaysum* documentation.

The receiver functions of the dipping and anisotropic lower crustal models shown in Figure 4c and d correspond to the ones shown in figure 3 of Porter et al. (2011). Specifically, both dipping and anisotropic layers are capable of converting seismic energy onto the transverse component, but the specific signature of amplitude variation with back-azimuth is distinct (although both show  $1-\theta$  patterns. On the transverse component, the dipping layer causes a broader symmetry pattern with a lower amplitude (Figure 4c), while the anisotropic layer produces high-amplitude conversions in a relatively narrow back-azimuth range (Figure 4d).

**Listing 3** Code to reproduce Figure 4 and figure 3 of Porter et al. (2011).

```
from pyraysum import Model, Geometry, Control
from pyraysum import run

# Lower-crustal dipping layer model
th = [20000, 5000, 0]
vp = [6400, 5800, 7800]
ps = [1.75, 1.74, 1.74]
dip = [0, 20, 20]
rho = 2800
st = 90

dipm = Model(
    th, rho, vp, vpv=ps, strike=st, dip=dip
)

# Lower crustal anisotropy model
ani = [0, -20, 0]
tr = [0, 180, 0]
pl = [0, 45, 0]
fl = [1, 0, 1]

anim = Model(
    th, rho, vp, vpv=ps,
    flag=fl, ani=ani, trend=tr, plunge=pl
)

# Evenly spaced back azimuths, fixed slowness
geom3 = Geometry(range(0, 360, 10), 0.06)

# Direct conversions, RTZ coordinate system
ctrl3 = Control(mults=0, rot="RTZ")

for model in [dipm, anim]:
    res = run(model, geom3, ctrl3, rf=True)
    res.filter(
        "rfs", "lowpass",
        freq=2., zerophase=True
    )

    model.plot_interfaces()
    res.plot("rfs", tmin=-0.5, tmax=4)
```

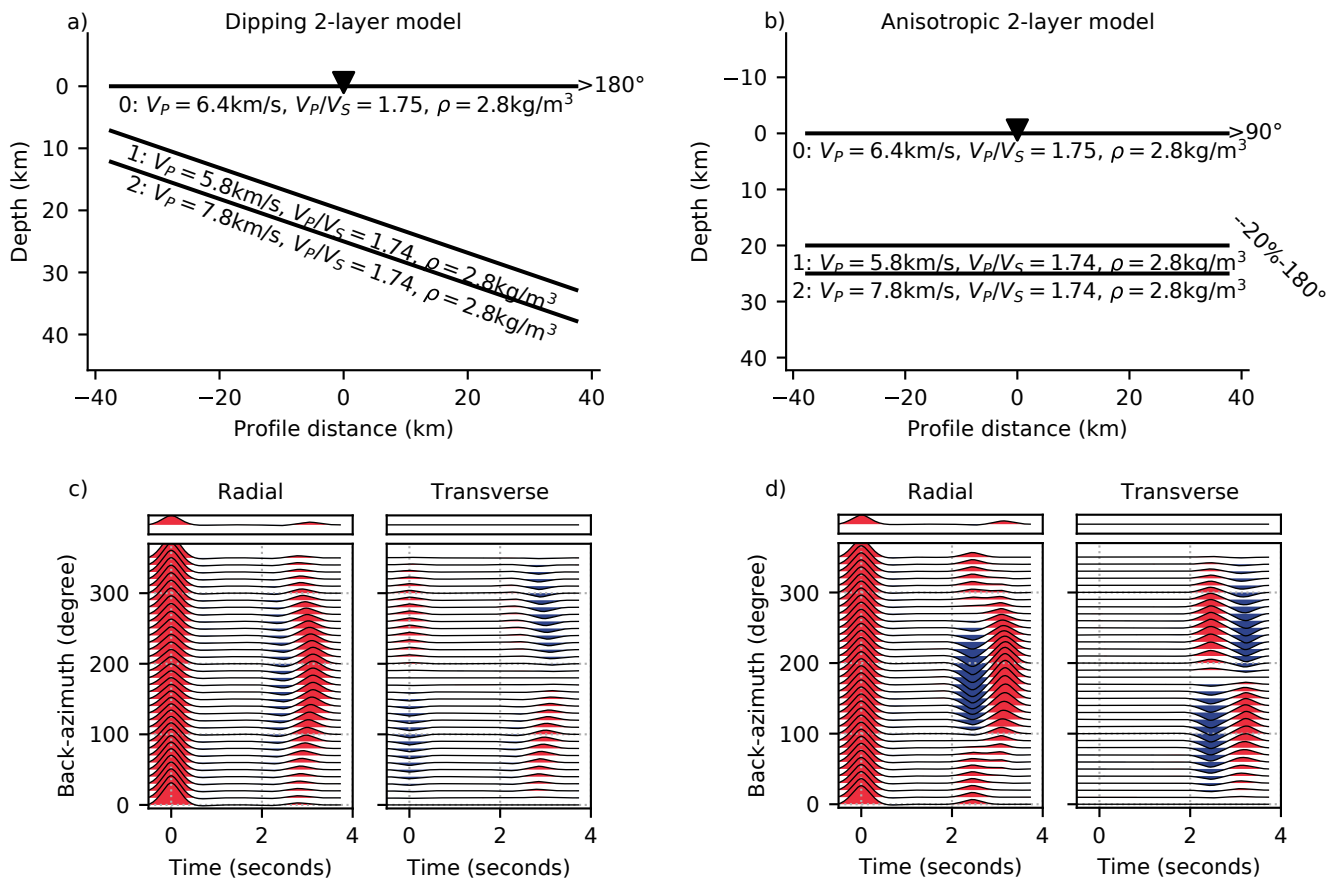


**Figure 4** Reproduction of figure 3 of Porter et al. (2011). (a) and (b) Layer geometry and properties. (c) and (d) Resulting receiver functions. The code that reproduces this figure is given in Listing 3.

## 4 Validation

We validate the synthetic seismograms created with *PyRaysum* by comparing them with those obtained using the matrix propagator method (Kennett, 2009; Thomson, 1997), as implemented in the *Telewavesim* package for Python (Audet et al., 2019), for the same seismic velocity models. The two test cases are the isotropic 1-layer case with free surface reflections (`mod1` in Listing 1; Figure 2) and the anisotropic lower crust case with direct conversions only (`anim` in Listing 3; Figure 4b and d). *Telewavesim* seismograms were generated using the code given in Listing 5. Note that *Telewavesim* lacks the capacity of synthesizing seismograms for dipping layers and inherently always includes all theoretical phase arrivals within the time window. Additionally, *Telewavesim* results do not provide a good infinite frequency approximation and therefore need to be filtered for comparison with *PyRaysum* results.

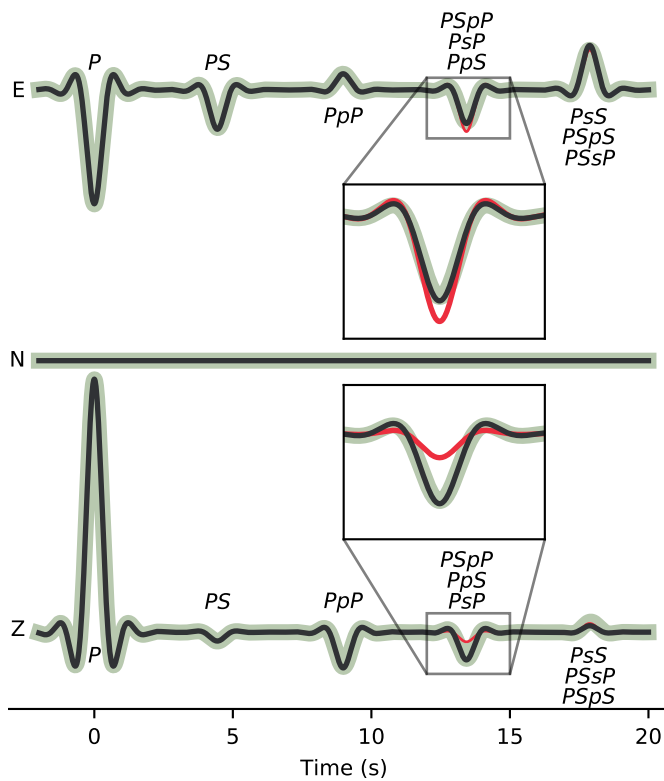
For the isotropic 1-layer model, the *Telewavesim* and *PyRaysum* traces agree with a cross-correlation coefficient of 0.9975, if multiples of the direct P-wave (first-order multiples) are considered (`mults=2`; Figure 5a). However, the amplitude of the *PpS* arrival differs noticeably. This is the case because, with the `mults=2` option, no second-order multiple is calculated. For instance, neither reflections of conversion (e.g., *PSpP*) nor conversions of reflections (e.g., *PsP*) are considered. As we will discuss below, this behaviour is deliberate, because

the implicit inclusion of these phases results in a large overhead for multi-layered models, leading to long run times and eventually segmentation faults. The limitation of `mults=2` to first-order multiples ensures that the phase with the largest amplitude is present in the synthetic seismograms.

In the present case, the free-surface reflection of the *P*-to-*S* Moho conversion *PSpP* contributes significantly to the amplitude of the *PpS* phase. Such equivalent phases can explicitly be included using the `Control.set_phaseList()` method. The unique set of phase descriptors present can be retrieved from a `Result` object and be used to compute the additional equivalent phases (Listing 4). With the inclusion of equivalent phases, the cross-correlation coefficient between the *Telewavesim* and *PyRaysum* seismograms improves to 0.9996 (Figure 5a).

For the anisotropic lower crust model (Figure 4, Listing 3), the *Telewavesim* and *PyRaysum* traces agree with a cross-correlation coefficient of 0.9996. Plotting of the `conversion_names` facilitates the interpretation of the complex converted wave forms in terms of conversions to fast and slow S-waves at the two subsurface interfaces (Figure 5b).

a) Isotropic 1-layer model



b) Anisotropic 2-layer model

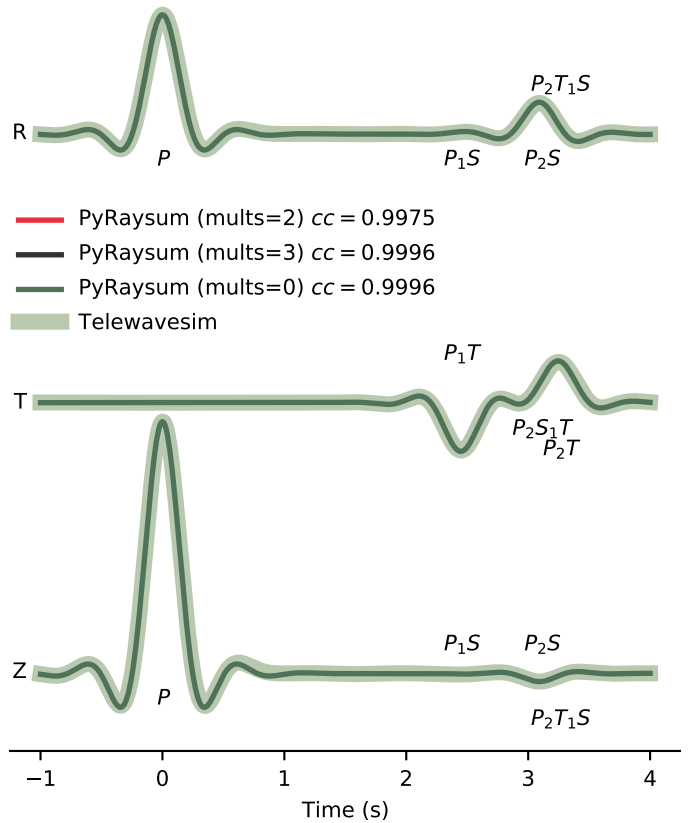


**Figure 5** Validation of the timing and amplitude of direct, converted and reflected seismic phases of *PyRaysum* (thin lines) against *Telewavesim* (thick lines). (a) Conversions and multiples in an isotropic 1-layer model (Figure 2, Listing 1); 1 Hz low-pass filter applied. (b) Direct conversions in an anisotropic lower crust model (Figure 4b and d, Listing 3). Phase nomenclature as in Section 2.2. ENZ: East, North, Vertical seismogram components. RTZ: Radial, Transverse, Vertical seismogram components.

## 5 Performance

We compared the run times of typical calls to *Raysum* with comparable calls to *PyRaysum*, as well as different processing options of *PyRaysum*, using an AMD EPYC™3 GHz Central Processing Unit.

We first tested the run time of the current *Raysum* version 1.2 with input models consisting of 1 to 7 layers over a half-space, for 24 rays, calculating all first order mul-

**Listing 4** Code illustrating the use of equivalent phases. Definitions of Listing 1 are assumed.

```
# Get descriptors from seismogram
descriptors = res1.descriptors()

# Add equivalent phases
# Implicitly sets Control.mults=3
ctrl1.set_phaselist(
    descriptors, equivalent=True
)

# Due east incidence
geom4 = Geometry(90, 0.06)

# Black seismogram of Figure 5a
res4 = run(mod1, geom4, ctrl1)
```

tiples (`mults=2`). The model, geometry and parameter files were read from disk; seismic traces, arrival times and phase descriptor files were written to disk. The computation completed in about 800 ms for the single layer model with a factorial increase to about 5 s for the 7 layer model (blue line in Figure 6). At 8 layers, *Raysum* encountered a segmentation fault, because the number of computed phases exceeded the maximum `maxph`, which is defined during compilation. Using *PyRaysum*, the same results can be obtained faster. With *NumPy* array output and an otherwise identical configuration, the 1 layer model completed in 70 ms and the 7 layer model in 2.1 s (teal line in Figure 6). These numbers convert to a 2- to 11-fold decrease in computation time, primarily because the in-/output overhead is avoided.

We now illustrate the computational cost of the treatment of phase combinations (setting of `Control.mults`) and the overhead of handling the metadata-rich *ObsPy* objects against the bare *NumPy* array. We use the *ObsPy*-based receiver function computation and filtering provisions as given in Listing 6 and measure the run time of Listing 6 with different options for `Control.mults`:

**Obs-M2-F-RF** Compute all conversions and first order multiples: `ctrl6 = Control(mults=2)`

**Obs-M0-F-RF** Only compute direct conversions:  
`ctrl6 = Control(mults=0)`

**Obs-M3-F-RF** Only compute two explicit phases:  
 the direct  $P$  wave and one  $P$ -to- $S$  conversion:  
`ctrl6.set_phaselist(["1P0P", "1P0S"])`  
 (for the 1-layer case). This implicitly sets  
`ctrl6.mults=3`.

The pink-shaded lines in Figure 6 illustrate the run time of Listing 6 with increasing number of layers in the model. When all conversions and multiples of all layers are computed (*Obs-M2-F-RF*), the run time increases factorially from about 200 ms for a one-layer model to 6.3 seconds for 7 layers. When only forward conversions are considered (*Obs-M0-F-RF*), the factorial increase is less steep. Explicitly fixing the number of rays to be computed (*Obs-M3-F-RF*) yields a constant run time, as expected. The likely small increase due to increased number of ray segments is smaller than the precision of our time measurement.

Run times on the order of a second are usually acceptable when executing code a few times manually. For frequent and automatic calls that do not require bookkeeping of metadata, results can be obtained faster by directly calling the Fortran routine `run_bare()`. We next illustrate the computational cost of three *NumPy*-based post-processing options, keeping the number of phases constant as in the last case examined above. The post processing steps timed are (Listing 7):

**Num-M3-F-RF** Compute seismograms. Then compute receiver functions through spectral division and filter them using `filtered_rf_array()`.

**Num-M3-F** Compute seismograms. Filter them using `filtered_array()`.

**Num-M3** Only compute synthetic seismograms.

In Listing 7, `rfarray` holds the processed data. It is allocated once before the (possibly subsequent) calls to `filtered_rf_array` or `filtered_array`.

For all three cases, run time is constant with respect to the number of model layers (green-shaded lines in Figure 6). Compared to the *ObsPy*-based post processing, time spent for filtering and spectral division (*Num-M3-F-RF*) is approximately halved, with only 100 instead of 200 ms, implying that as much time is required for bookkeeping. Sparing spectral division (*Num-M3-F*) saves about 1/5th of run time, or 20 ms in the present example. Filtering is computationally cheap, taking only about 1/25th of time, or 5 ms (*Num-M3*).

## 6 Outlook and Future Work

With the time-efficient, *NumPy*-based post-processing, *PyRaysum* can be used as a forward code in parameter estimation problems. For example, the common problem of finding the optimal crustal thickness and bulk  $V_P/V_S$  ratio from the time and amplitude of the Moho conversion and reverberations in receiver functions (e.g. [Zhu and Kanamori, 2000](#)) can be re-formulated as a

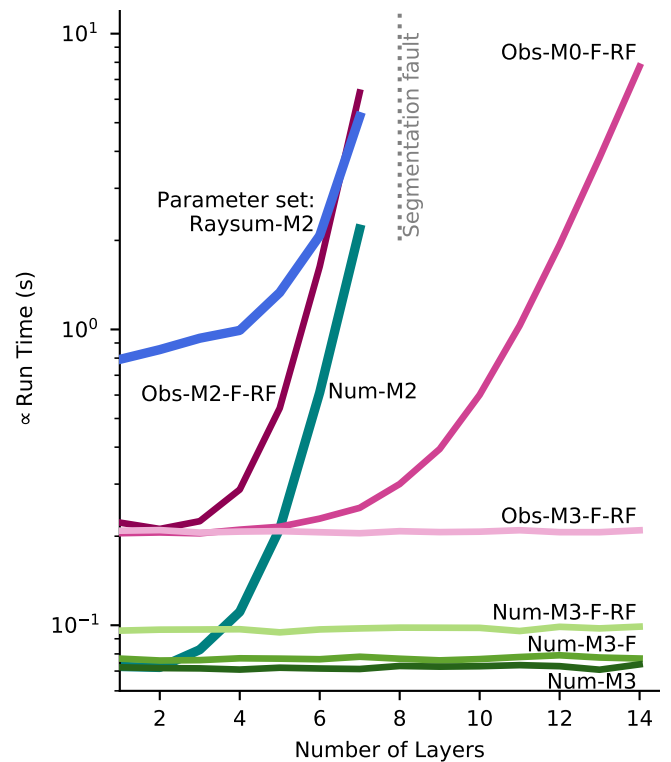


**Figure 6** Runtime of *Raysum* and different configurations of *PyRaysum* as a function of numbers of layers in the model. The parameter sets correspond to the following configurations: *Raysum*: Call the *Raysum* binary `seis-spread` from the command line; Parse program in- and output through files. *Obs*: execute `prs.run` and use *Result* class methods for post-processing (Listing 6). *Num*: execute `fraysum.run_bare()` and use *NumPy* array-based post-processing functions (Listing 7). M0, M2, M3: `mults` set to 0, 2, or 3. F: filter. RF: compute receiver functions.

minimum misfit problem and be generalized to multi-layered models. First tests indicate that, e.g., *SciPy*'s `dual_annealing()` function can find a minimum misfit model from teleseismic receiver functions for the thickness,  $V_S$ , and  $V_P/V_S$  of three layers representative for the continental crust and subducting slab of the Cascadia subduction zone within a few hours. Automatic phase labels (Figures 2 and 5) can help to identify more multiples in complex receiver functions and facilitate a more thorough understanding of the scattered wave field.

Anisotropy is currently parameterized as a single parameter,  $ani$  (Equation 1). Internally, *Raysum* handles anisotropy in its most general form using the Christoffel equation. This in principle allows to explore other theoretical crystal symmetry classes (e.g. general hexagonal, orthorhombic), as well as anisotropy predicted and measured for specific minerals and rocks (e.g. [Brownlee et al., 2017](#)), which can be implemented through a new definition and internal handling of the *Model* class.

## 7 Conclusion

*PyRaysum* is a modern and fast incarnation of *Raysum* ([Frederiksen and Bostock, 2000](#)), the popular algorithm

to compute seismograms that result from the plane wave propagation through dipping, anisotropic, layered media. New features include bypassing hard disk read-write operations, automatic labeling of seismic phases, easy definition of explicit phase lists, inclusion of equivalent phases, *ObsPy* integration, efficient receiver function post processing, and interactive manipulation of subsurface models. With these improvements, *PyRaysum* makes it possible to play with receiver functions in a simple and efficient Python environment, as well as to invert for subsurface properties using state-of-the-art inverse modeling algorithms.

## ACKNOWLEDGMENTS

The authors thank Andrew Frederiksen for extensive discussion, and for his continued work on *Raysum*; and Michael Bostock for discussion. First and foremost, please cite their work (Frederiksen and Bostock, 2000) when using *PyRaysum*. The comments of two anonymous reviewers helped to improve the manuscript and the initial major release of *PyRaysum*. WB was located on the traditional, ancestral, and unceded territories of the Musqueam People while performing this research. PA acknowledges and respects that his workplace stands on unceded Algonquin territory. This work is funded by the German Research Foundation, grant BL 1758/1-1, and by the Natural Science and Engineering Research Council of Canada, Discovery grant RGPIN-2018-03752. *PyRaysum* relies on open-source software, namely *ObsPy* (Krischer et al., 2015), *NumPy* (Harris et al., 2020), and *SciPy* (Virtanen et al., 2020). Figures were created with *Matplotlib* (Hunter, 2007).

## Code availability

*PyRaysum* is open-source software and is under active development on *GitHub* (<https://github.com/paudetseis/PyRaysum>, last accessed January 2023). A snapshot of the most recent version 1.0.0 is hosted on zenodo (Audet and Bloch, 2022). The full documentation is included with the current snapshot and online at <https://paudetseis.github.io/PyRaysum/index.html>. *Raysum* is available at <https://home.cc.umanitoba.ca/~frederik/Software/>.

## References

- Audet, P. and Bloch, W. PyRaysum: Software for modeling ray-theoretical body-wave propagation. Dec. 2022. doi: 10.5281/zenodo.7468301.
- Audet, P. and Bürgmann, R. Possible control of subduction zone slow-earthquake periodicity by silica enrichment. *Nature*, 510 (7505):389–392, jun 2014. doi: 10.1038/nature13391.
- Audet, P., Thomson, C., Bostock, M., and Eulenfeld, T. Telewavesim: Python software for teleseismic body wave modeling. *Journal of Open Source Software*, 4(44):1818, dec 2019. doi: 10.21105/joss.01818.
- Brownlee, S. J., Schulte-Pelkum, V., Raju, A., Mahan, K., Condit, C., and Orlandini, O. F. Characteristics of deep crustal seismic anisotropy from a compilation of rock elasticity tensors and their expression in receiver functions. *Tectonics*, 36(9):1835–1857, sep 2017. doi: 10.1002/2017tc004625.
- Cassidy, J. F. and Ellis, R. M. S-wave velocity structure of the Northern Cascadia subduction zone. *Journal of Geophysical Research: Solid Earth*, 98(B3):4407–4421, mar 1993. doi: 10.1029/92jb02696.
- Frederiksen, A. W. and Bostock, M. G. Modelling teleseismic waves in dipping anisotropic structures. *Geophysical Journal International*, 141(2):401–412, may 2000. doi: 10.1046/j.1365-246x.2000.00090.x.
- Harris, C. R., Millman, K. J., van der Walt, S. J., Gommers, R., Virtanen, P., Cournapeau, D., Wieser, E., Taylor, J., Berg, S., Smith, N. J., Kern, R., Picus, M., Hoyer, S., van Kerkwijk, M. H., Brett, M., Haldane, A., del Río, J. F., Wiebe, M., Peterson, P., Gérard-Marchant, P., Sheppard, K., Reddy, T., Weckesser, W., Abbasi, H., Gohlke, C., and Oliphant, T. E. Array programming with NumPy. *Nature*, 585(7825):357–362, Sept. 2020. doi: 10.1038/s41586-020-2649-2.
- Hunter, J. D. Matplotlib: A 2D graphics environment. *Computing in Science & Engineering*, 9(3):90–95, 2007. doi: 10.1109/M-CSE.2007.55.
- Kennett, B. *Seismic Wave Propagation in Stratified Media*. ANU Press, 2009. doi: 10.26530/oapen\_459524.
- Kennett, B. L. N. The removal of free surface interactions from three-component seismograms. *Geophysical Journal International*, 104(1):153–154, jan 1991. doi: 10.1111/j.1365-246x.1991.tb02501.x.
- Krischer, L., Megies, T., Barsch, R., Beyreuther, M., Lecocq, T., Caudron, C., and Wassermann, J. ObsPy: a bridge for seismology into the scientific Python ecosystem. *Computational Science & Discovery*, 8(1):014003, may 2015. doi: 10.1088/1749-4699/8/1/014003.
- Kumar, P., Yuan, X., Kumar, M. R., Kind, R., Li, X., and Chadha, R. K. The rapid drift of the Indian tectonic plate. *Nature*, 449(7164): 894–897, oct 2007. doi: 10.1038/nature06214.
- Levin, V. and Park, J. P-SH conversions in a flat-layered medium with anisotropy of arbitrary orientation. *Geophysical Journal International*, 131(2):253–266, nov 1997. doi: 10.1111/j.1365-246x.1997.tb01220.x.
- Lombardi, D., Braunmiller, J., Kissling, E., and Giardini, D. Moho depth and Poisson's ratio in the Western-Central Alps from receiver functions. *Geophysical Journal International*, 173(1):249–264, apr 2008. doi: 10.1111/j.1365-246x.2007.03706.x.
- Nicholson, T., Bostock, M., and Cassidy, J. F. New constraints on subduction zone structure in northern Cascadia. *Geophysical Journal International*, 161(3):849–859, jun 2005. doi: 10.1111/j.1365-246x.2005.02605.x.
- Porter, R., Zandt, G., and McQuarrie, N. Pervasive lower-crustal seismic anisotropy in Southern California: Evidence for under-plated schists and active tectonics. *Lithosphere*, 3(3):201–220, jun 2011. doi: 10.1130/l126.1.
- Saul, J., Kumar, M. R., and Sarkar, D. Lithospheric and upper mantle structure of the Indian shield, from teleseismic receiver functions. *Geophysical Research Letters*, 27(16):2357–2360, aug 2000. doi: 10.1029/1999gl011128.
- Schneider, F., Yuan, X., Schurr, B., Mechie, J., Sippl, C., Haberland, C., Minaev, V., Oimahmadov, I., Gadoev, M., Radjabov, N., Abdybachev, U., Orunbaev, S., and Negmatullaev, S. Seismic imaging of subducting continental lower crust beneath the Pamir. *Earth and Planetary Science Letters*, 375:101–112, aug 2013. doi: 10.1016/j.epsl.2013.05.015.
- Schulte-Pelkum, V., Monsalve, G., Sheehan, A., Pandey, M. R., Sapkota, S., Bilham, R., and Wu, F. Imaging the Indian subcontinent beneath the Himalaya. *Nature*, 435(7046):1222–1225, jun 2005. doi: 10.1038/nature03678.
- Selway, K., Ford, H., and Kelemen, P. The seismic mid-lithosphere discontinuity. *Earth and Planetary Science Letters*, 414:45–57, mar 2015. doi: 10.1016/j.epsl.2014.12.029.
- Sherrington, H. F., Zandt, G., and Frederiksen, A. Crustal fabric in the Tibetan plateau based on waveform inversions for seismic anisotropy parameters. *Journal of Geophysical Research: Solid Earth*, 109(B2), feb 2004. doi: 10.1029/2002jb002345.
- Sodoudi, F., Yuan, X., Kind, R., Heit, B., and Sadidkhoy, A. Evidence for a missing crustal root and a thin lithosphere beneath the Central Alborz by receiver function studies. *Geophysical Journal International*, 177(2):733–742, may 2009. doi: 10.1111/j.1365-246x.2009.04115.x.
- Thomson, C. Modelling surface waves in anisotropic structures i. theory. *Physics of the Earth and Planetary Interiors*, 103(3-4): 195–206, nov 1997. doi: 10.1016/s0031-9201(97)00033-2.
- Virtanen, P., Gommers, R., Oliphant, T. E., Haberland, M., Reddy, T., Cournapeau, D., Burovski, E., Peterson, P., Weckesser, W., Bright, J., van der Walt, S. J., Brett, M., Wilson, J., Millman, K. J., Mayorov, N., Nelson, A. R. J., Jones, E., Kern, R., Larson, E., Carey, C. J., Polat, İ., Feng, Y., Moore, E. W., VanderPlas, J., Laxalde, D., Perktold, J., Cimrman, R., Henriksen, I., Quintero, E. A., Harris, C. R., Archibald, A. M., Ribeiro, A. H., Pedregosa, F., van Mulbregt, P., and SciPy 1.0 Contributors. SciPy 1.0: Fundamental Algorithms for Scientific Computing in Python. *Nature Methods*, 17:261–272, 2020. doi: 10.1038/s41592-019-0686-2.
- Zhu, L. and Kanamori, H. Moho depth variation in southern California from teleseismic receiver functions. *Journal of Geophysical Research: Solid Earth*, 105(B2):2969–2980, feb 2000. doi: 10.1029/1999jb900322.

## A Synthetic seismograms for cross validation

**Listing 5** Code to generate *Telewavesim* seimograms for validation (Figure 5). Assumes definitions of Listings 1 and 3

```
from telewavesim import utils as tws

baz = 90 # Back-azimuth
slow = 0.06 # Slowness
npts = 4500 # Samples
dt = 0.01 # Sampling Interval
anid = {1: "iso", 0: "tri"} # Anisotropy ID

# Isotropic 1-layer model
tmodi = tws.Model(
    mod1["thickn"] * 1e-3,
    mod1["rho"],
    mod1["vp"] * 1e-3,
    mod1["vs"] * 1e-3,
)

twi = tws.run_plane(
    tmodi, slow, npts, dt, baz
)

# Anisotropic 2-layer model
tmoda = tws.Model(
    anim["thickn"] * 1e-3,
    anim["rho"],
    anim["vp"] * 1e-3,
    anim["vs"] * 1e-3,
    [anid[f] for f in anim["flag"]],
    anim["ani"],
    anim["trend"],
    anim["plunge"],
)

# Run Telewavesim
twa = tws.run_plane(
    tmoda, slow, npts, dt, baz
)
```

## B Performance of *ObsPy*-based post-processing

**Listing 6** Template for *ObsPy*-based receiver function computation and post processing. Assumes definitions of Listing 1. For performance testing, `Control.mults` was chosen as described in Section 5.

```
ctrl6 = Control(mults=0) # See Section 5
for _ in range(13):
    print(len(mod1), "layers", end="... ")
    res6 = run(mod1, geom1, ctrl6)
    res6.calculate_rfs()
    res6.filter(
        "rfs",
        "bandpass",
        freqmin=0.05,
        freqmax=0.5,
        zerophase=True,
        corners=2,
    )
    print("Done!")
    # Split topmost layer in two
    mod1.split_layer(0)
```

## C Performance of *NumPy*-based post-processing

**Listing 7** The three *NumPy*-based performance test cases spelled out for the 1-layer example of Listing 1.

```
from pyraysum import frs
from fraysum import run_bare
cases = ["Num-M3-F-RF", "Num-M3-F", "Num-M3"]

fmin = 0.05
fmax = 0.5 # Filter corners in Hz
ctrl1.set_phaselist(["1P0P", "1P0S"])
ctrl1.rot = "PVH" # P-V-H coordinates
rfarray = frs.make_array(geom1, ctrl1)

for case in cases:
    array = run_bare(
        *mod1.parameters,
        *geom1.parameters,
        *ctrl1.parameters,
    )

    if case == "Num-M3-F-RF":
        frs.filtered_rf_array(
            array,
            rfarray,
            geom1.ntr,
            ctrl1.npts,
            ctrl1.dt,
            fmin,
            fmax,
        )

    if case == "Num-M3-F":
        frs.filtered_array(
            array,
            rfarray,
            geom1.ntr,
            ctrl1.npts,
            ctrl1.dt,
            fmin,
            fmax,
        )
```